## Supplementary Material for:

# CoCEST: Cobalt(II) Amide-Appended ParaCEST MRI Contrast Agents

Sarina J. Dorazio, Abiola O. Olatunde, Joseph A. Spernyak, Janet R. Morrow

Department of Chemistry, State University of New York, University at Buffalo, Amherst, NY 14260, United States
Department of Cell Stress Biology, Roswell Park Cancer Institute, Buffalo, NY 14263, United States

**Table of Contents** **Page**

**Materials & Methods**

*Instrumentation.* Varian Inova 400 MHz and Inova 500 MHz NMR spectrometers were used to collect $^{1}$H NMR spectra. Evans' measurements of magnetic susceptibility and CEST data were acquired on a Varian Inova 500 MHz spectrometer. ThermoFinnigan LCQ Advantage IonTrap LC/MS equipped with a Surveyor HPLC system was used to collect mass spectral data. $Cu^{II}$ displacement assay absorbance measurements were recorded every 60 s with a Beckman-Coulter DU 800 UV-vis spectrophotometer connected to a Peltier Temperature Controller. A Thermo Scientific Orion 9826BN NMR micro pH electrode connected to a SympHony SB20 pH meter was used to obtain pH measurements.

*Determination of magnetic moment.* The effective magnetic moment ($\mu_{eff}$) was calculated by using the Evans' method.[1,2] 5 mM $Co^{II}$ complex and 5 % t-butanol by volume was placed in a NMR insert while the outer NMR tube contained 5 % by volume t-butanol in $D_2O$. The concentration of the $Co^{II}$ complexes was determined by integration of the proton resonances of the complex relative to the 3-(trimethylsilyl)-1-propanesulfonic acid standard and/or by preparation of stock solutions of complex. The $\mu_{eff}$ was calculated at 298 K (T) from NMR data, measured in triplicate, and monitored over a period of 72 h using the following equations:

$$\chi_g = (-3\Delta f)/(4\pi fm) + \chi_0 + [\chi_0 (d_0-d_s)]/m \quad \textbf{eq.S1}$$

$$\mu_{eff} = 2.84 (\chi_m T)^{1/2} \quad \textbf{eq. S2}$$

The mass susceptibility of solute ($\chi_g$) was calculated by obtaining the observed frequency shift of the reference ($\Delta f$ ) in Hz, the spectrometer frequency (f) in Hz, the mass of the substance per $cm^3$ of solution (m), and the mass susceptibility of solvent $D_2O$ ($\chi_0$= -0.6466 x $10^{-6}$ $cm^3/g$ ).[3] The last term is neglected due to the minimal contribution to mass susceptibility of solute, in

which $d_o$ is density of the solvent and $d_s$ is density of the solution in g/cm$^3$. The molar susceptibility ($\chi_m$) is the product of $\chi_g$ multiplied by the molecular weight of the $Co^{II}$ complex.

*Monitoring dissociation of complex over time*. Dissociation of the $Co^{II}$ complexes was monitored *via* $^1$H NMR spectroscopy of samples incubated at 37 $^o$C over a period of 12 h. To monitor acid dissociation, samples contained 10 mM $Co^{II}$ complex, 100 mM NaCl, and 3-5 mM 3-(trimethylsilyl)-1-propanesulfonic acid sodium salt as a standard at pD 3.5 – 3.9. To assess the complexes in the presence of biologically relevant anions, solutions contained 10 mM $Co^{II}$ complex, 100 mM NaCl, 0.40 mM $Na_2HPO_4$ , 25 mM $K_2CO_3$, and 5 mM 3-(trimethylsilyl)-1-propanesulfonic acid sodium salt as a standard. Generally, 1024 transients were collected for each spectrum.

*Displacement by Cu$^{II}$*. The displacement of $Co^{II}$ from the complex by $Cu^{II}$ was monitored over a period of 3 h at 37 °C by UV-vis. Samples contained 200 μM $Co^{II}$ complex, 10 mM MES buffer pH 5.5 and 1, 4, or 10 equivalents of $CuCl_2$. The formation of the $Cu^{II}$ complexes was monitored at 264 nm, 286 nm, 312 nm and 310 nm for $[Cu(1)]^{2+}$, $[Cu(44)]^{2+}$, $[Cu(2)]^{2+}$, and $[Cu(3)]^{2+}$, respectively. A previously reported procedure was followed.[4]

*CEST spectroscopy.* CEST data were acquired with a presaturation pulse power ($B_1$) of 1000 Hz (24 μT) applied for 2 s at 37 $^o$C. In general, 12 transients were acquired for each CEST spectrum. Data were acquired in 0.5 or 1 ppm increments and plotted as normalized water signal intensity ($M_z/M_o$ %) against frequency offset (ppm) to produce a CEST spectrum. Samples contained 10 mM $Co^{II}$ complex, 20 mM buffer, and 100 mM NaCl in a NMR insert. To lock the sample, $d_6$-DMSO was placed in the outer NMR tube.

*Determination of exchange rate constants.* Exchange rate constants were calculated following a previously reported procedure.[5] Measurements of on-resonance ($M_z$) and off-

resonance ($M_o$) were acquired at different presaturation pulse powers between 350-1000 Hz (8 – 24 μT) applied for 4 s at 37 $^oC$. The exchange rate constant ($k_{ex}$) is calculated from the x-intercept from the plot of $M_z/(M_o-M_z)$ against $1/\omega_1^2$ ($\omega_1$ in rad/s). Samples contained 10 mM $Co^{II}$ complex, 20 mM HEPES pH 7.4, and 100 mM NaCl.

*CEST Imaging.* CEST MR images were acquired on a 4.7 T preclinical MR scanner using a 35 mm transceiver coil (ParaVision 3.0.2, Bruker Biospin, Billerica, MA) as detailed elsewhere.[2] Two spoiled gradient-echo images (TE/TR = 2.1/5010 ms, flip angle = 90$^o$) were acquired at 37 °C after employing a pulse train comprised of five Gauss pulses (12 μT for 1 s each, interpulse delay of 200 μs) applied symmetrically about the bulk water resonance. To address concerns of magnetic field ($B_0$) inhomogeneity affecting the offset frequency of the samples during MR imaging, the $B_0$-field was mapped using a cylindrical phantom of water and the imaging phase data at isocenter was examined to determine in-plane homogeneity. The $B_0$ field strength ranged < 0.65 ppm over the field of view and therefore $B_0$-field inhomogeneity was not anticipated to affect PARACEST offset frequencies to any significant degree. Image processing was carried out using in-house software algorithms developed in MATLAB (MathWorks, Natick, MA). Each image was normalized to the mean intensity of the buffer/salt phantom, and the mean signal intensity of each compound was sampled. The percent change in signal, or CEST effect (CE), was calculated as: $CE = (1 - SI_{on}/SI_{off}) \times 100$, where $SI_{on}$ and $SI_{off}$ represent the mean signal intensity of each sample with the presaturation pulse applied on- and off-resonance of the exchangeable protons, respectively. CEST images were calculated by determining CE on a pixel-by-pixel basis in MATLAB. To improve visualization of the CEST effect, images were filtered with a spatial averaging filter (kernel size = 5 x 5), background noise was removed using a binary mask of the samples, and a 'hot-iron' color lookup table was

applied. For determining the ratio of CEST effect at 112 ppm vs. 95 ppm, CEST images were acquired with an identical presaturation pulse train as above but image encoding was carried out using an FID-FISP acquisition to reduce acquisition times. Imaging parameters for the FID-FISP acquisition include: matrix = 128 x 128, field of view = 3.2 x 3.2 cm, TE/TR = 1.5/3.0 ms, flip angle = 90°, number of repetitions = 20. Processing was carried out as above with the exception that the 20 repetition image datasets were averaged together prior to normalization by the buffer signal intensity. Image acquisition time for the FID-FISP acquisition was 100 seconds for imaging at a single offset frequency resulting in a total of 300 s for acquiring image data with saturation pulses +112, +95 and -95 ppm. The experiment was repeated with three separate preparations of $[Co(3)]^{2+}$.

*$T_1/T_2$ Relaxivity.* Using serial dilutions, $T_1/T_2$ relaxivity values were determined at 4.7 T, 37 °C as previously described.[6] $T_1$ relaxation rate constants were measured using an inversion-recovery TrueFISP acquisition, while $T_2$ relaxation rate constants were measured using a multi-echo, Carr-Purcell-Meiboom-Gill spin-echo sequence with a fixed TR of 3000 ms and TE times ranging from 20-1200 ms. Non-linear regression analysis in MATLAB was used to calculate the $T_1$ and $T_2$ relaxation rate constants and relaxivities were then determined by linear regression fitting of the concentration vs. $T_1/T_2$ rate in Microsoft Excel.

*Materials*. All reagents were used without further purification. $CoCl_2 \cdot 6H_2O$ was purchased from Alfa Aesar. TACN was purchased from TCI America. Cyclen and Cyclam were purchased from Strem Chemicals.

*Synthesis.* Previously published procedures were followed for the syntheses of ligands 1, 2, 3, and 4.[7-11] In a typical preparation, the ligand was complexed with equimolar $CoCl_2 \cdot 6H_2O$ in ethanol at room temperature. The complexes were isolated as solids and dried under vacuum

to produce $[Co(1)]^{2+}$, $[Co(4)]^{2+}$, $[Co(2)]^{2+}$, and $[Co(3)]^{2+}$. **$[Co(1)]^{2+}$** was obtained as a pastel blue to periwinkle powder. Yield: 71 % ESI-MS: m/z = 179.8 (86 %) $[M/2]^+$, 358.2 (100 %) $[M – H]^+$, 394.0 (20 %) $[M + Cl]^+$. **$[Co(4)]^{2+}$** was obtained as a light purple powder. Yield: 80 % ESI-MS: *m/z* = 195.8 (100 %) $[M/2]^+$, 390.2 (57 %) $[M – H]^+$, 426.0 (54%) $[M + Cl]^+$. **$[Co(2)]^{2+}$** was obtained as a pastel blue powder. Yield: 91 % ESI-MS: m/z = 229.8 (100 %) $[M/2]^+$, 458.3 (72 %) $[M – H]^+$. **$[Co(3)]^{2+}$** was obtained as a pale pink to lavender powder. Yield: 90 % ESI-MS: m/z = 243.8 (100 %) $[M/2]^+$, 486.3 (56 %) $[M – H]^+$.

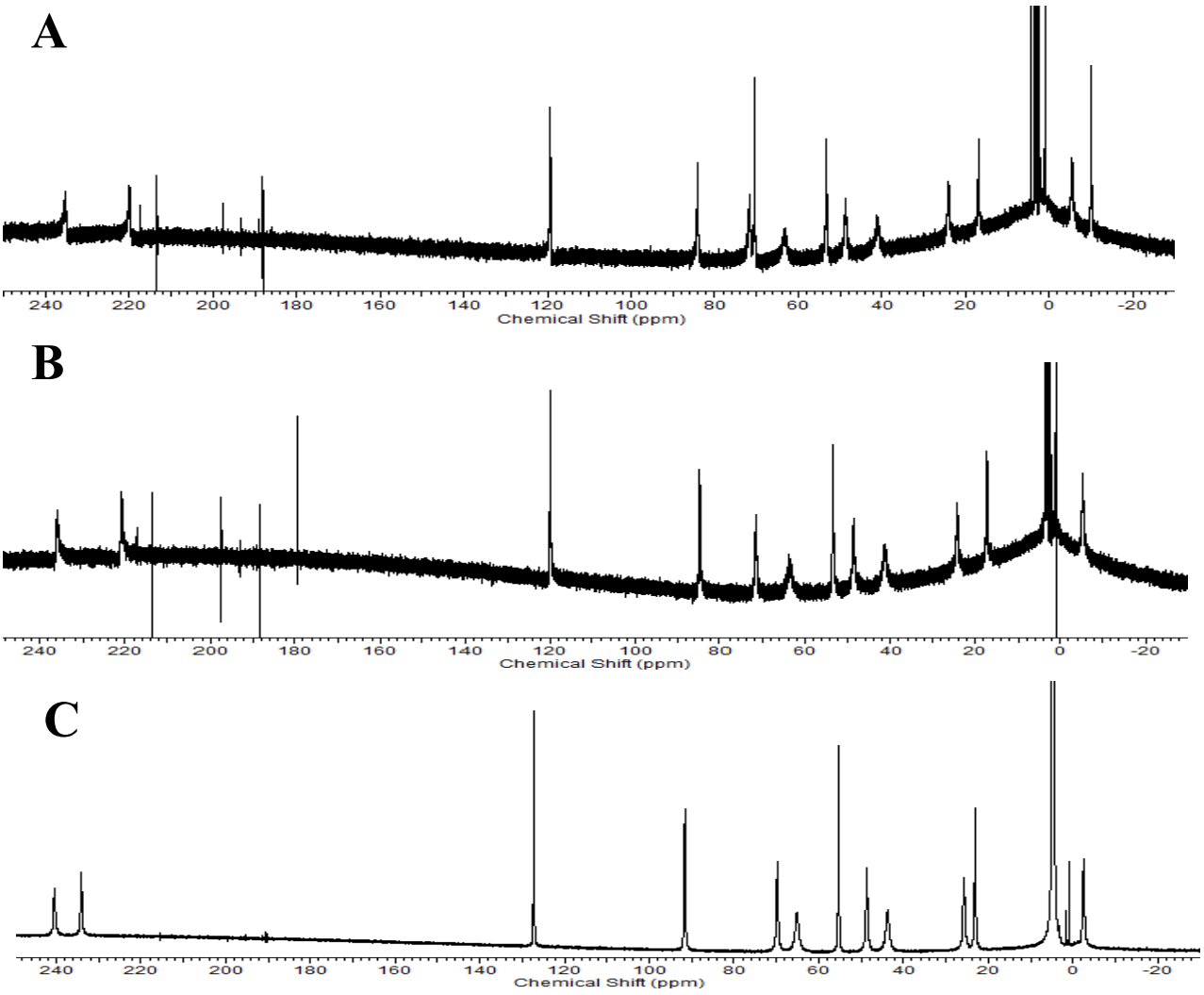


**Figure S1.** $^{1}$H NMR spectra of $[Co(4)]^{2+}$ in A) $d_6$-DMSO, B) $d_6$-DMSO + $D_2O$ C) $D_2O$.

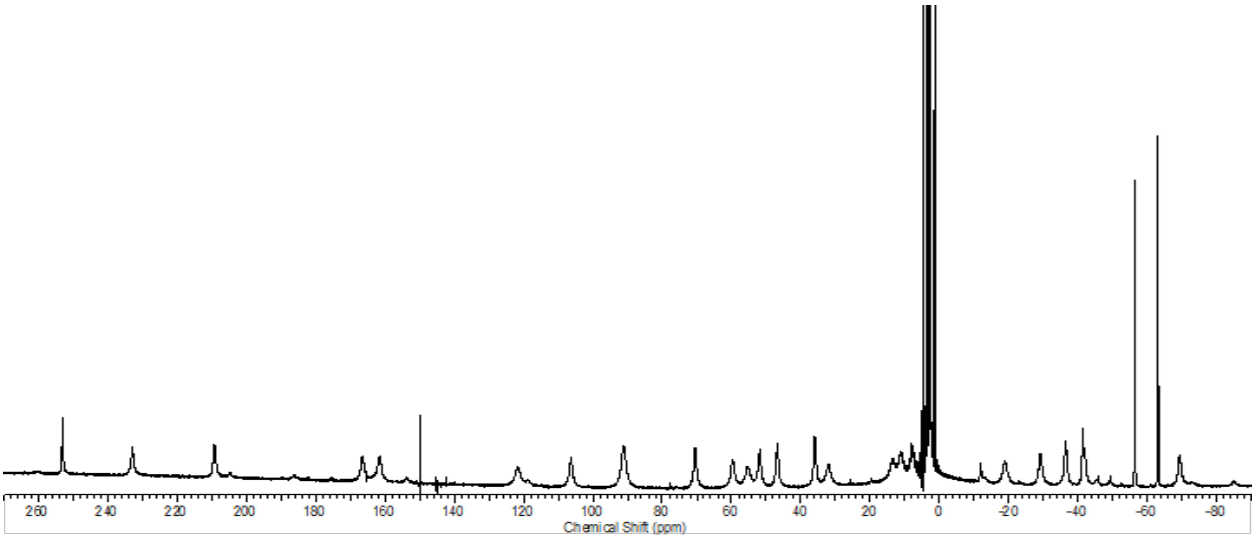


**Figure S2.** $^{1}$H NMR spectrum of $[Co(3)]^{2+}$ in $D_2O$.

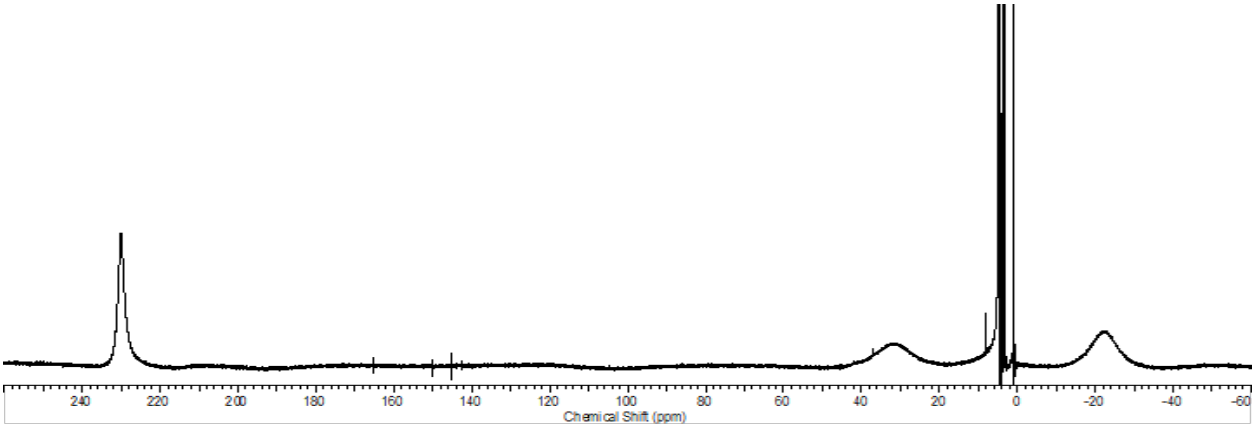


**Figure S3.** $^{1}$H NMR spectrum of $[Co(1)]^{2+}$ in $D_2O$.

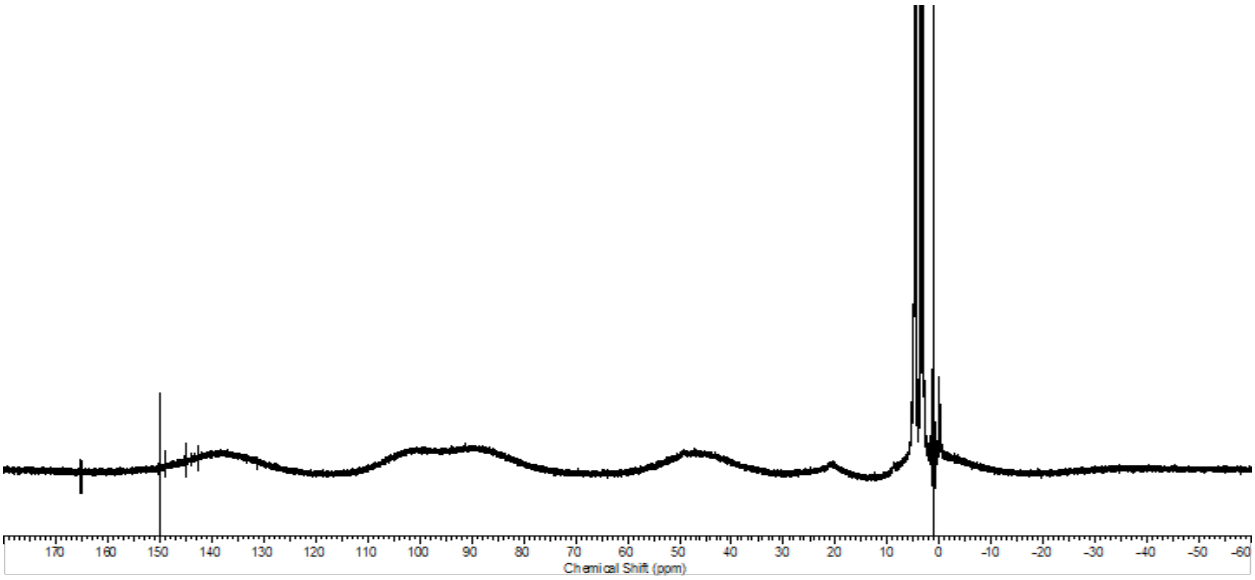


**Figure S4.** $^{1}$H NMR spectrum of $[Co(2)]^{2+}$ in $D_2O$.

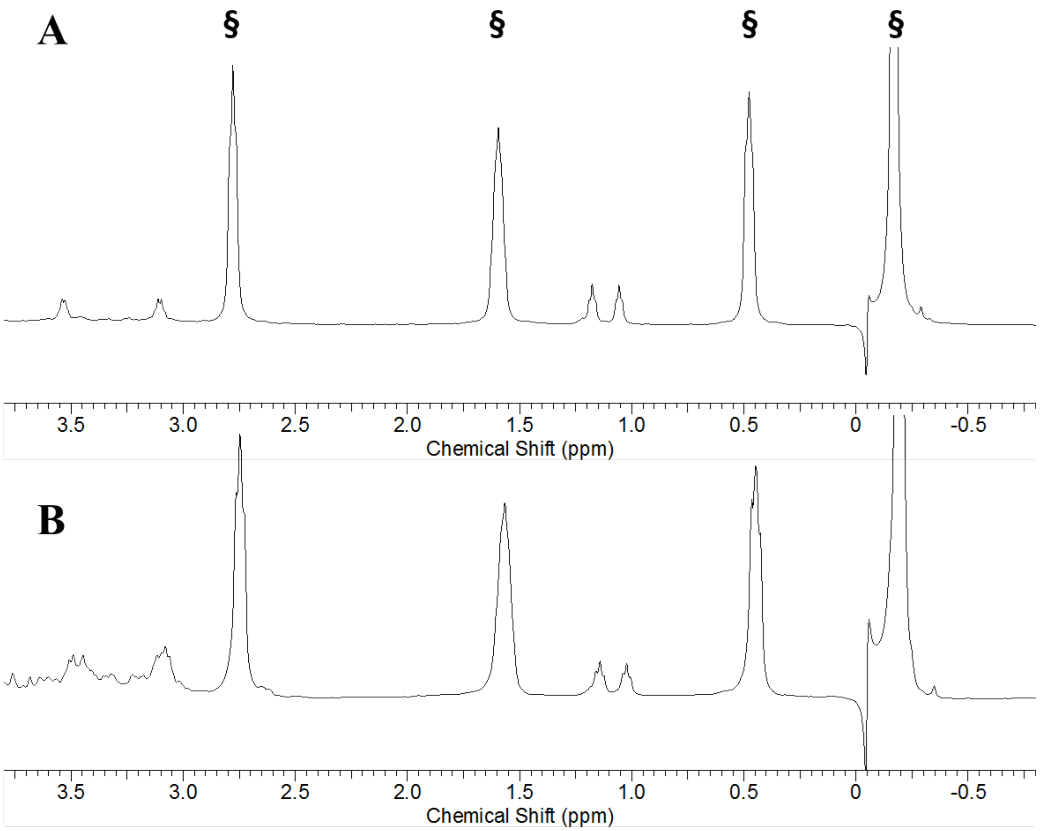


**Figure S5.** Diamagnetic region $^{1}$H NMR spectra of 10 mM $[Co(1)]^{2+}$,100 mM NaCl, 0.40 mM $Na_2HPO_4$, 25 mM $K_2CO_3$ in $D_2O$, pD 7.5 at 25 $^{o}$C (A) at 1 h (B) at 12 h after incubation at 37 $^{o}$C. Contains 5 mM 3-(trimethylsilyl)-1-propanesulfonic acid standard, indicated by §.

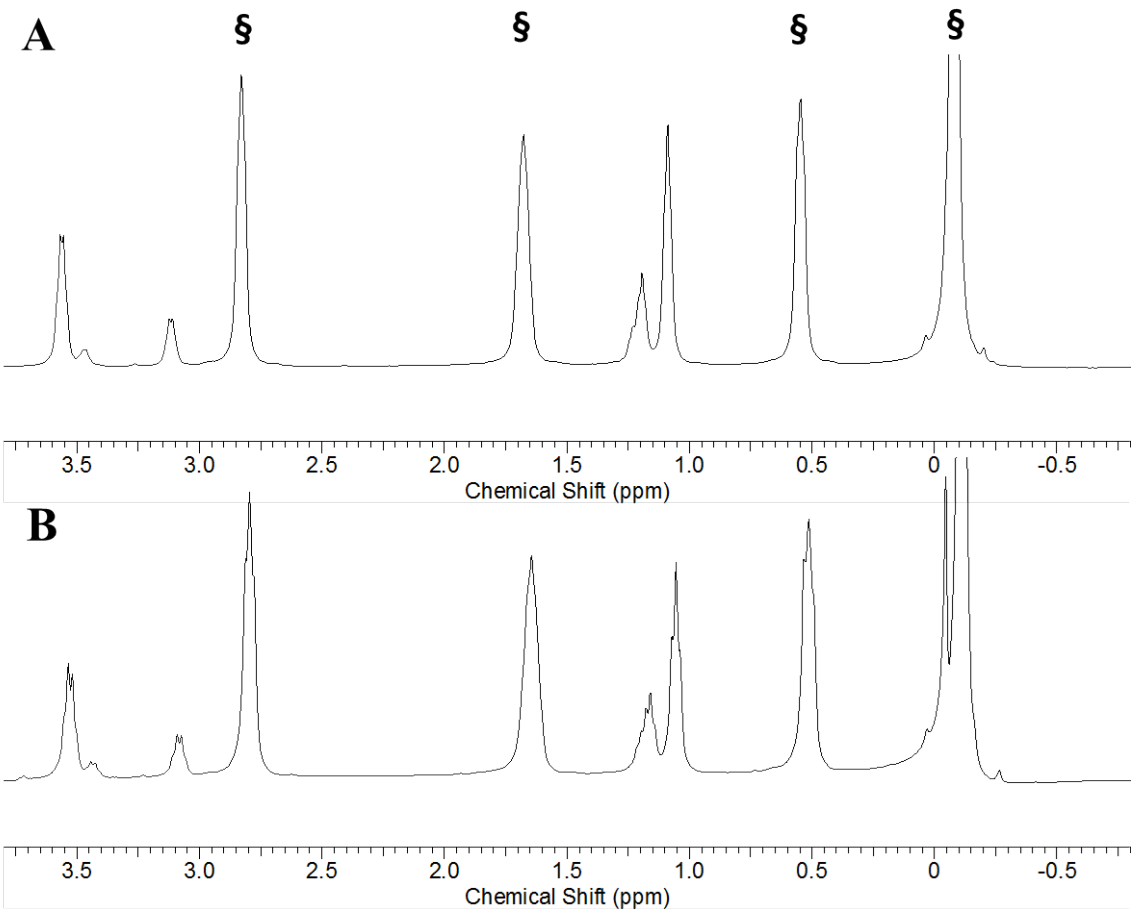


**Figure S6.** Diamagnetic region $^{1}$H NMR spectra of 10 mM $[Co(2)]^{2+}$,100 mM NaCl, 0.40 mM $Na_2HPO_4$, 25 mM $K_2CO_3$ in $D_2O$, pD 7.5 at 25 $^{o}$C (A) at 1 h (B) at 12 h after incubation at 37 $^{o}$C. Contains 5 mM 3-(trimethylsilyl)-1-propanesulfonic acid standard, indicated by §.

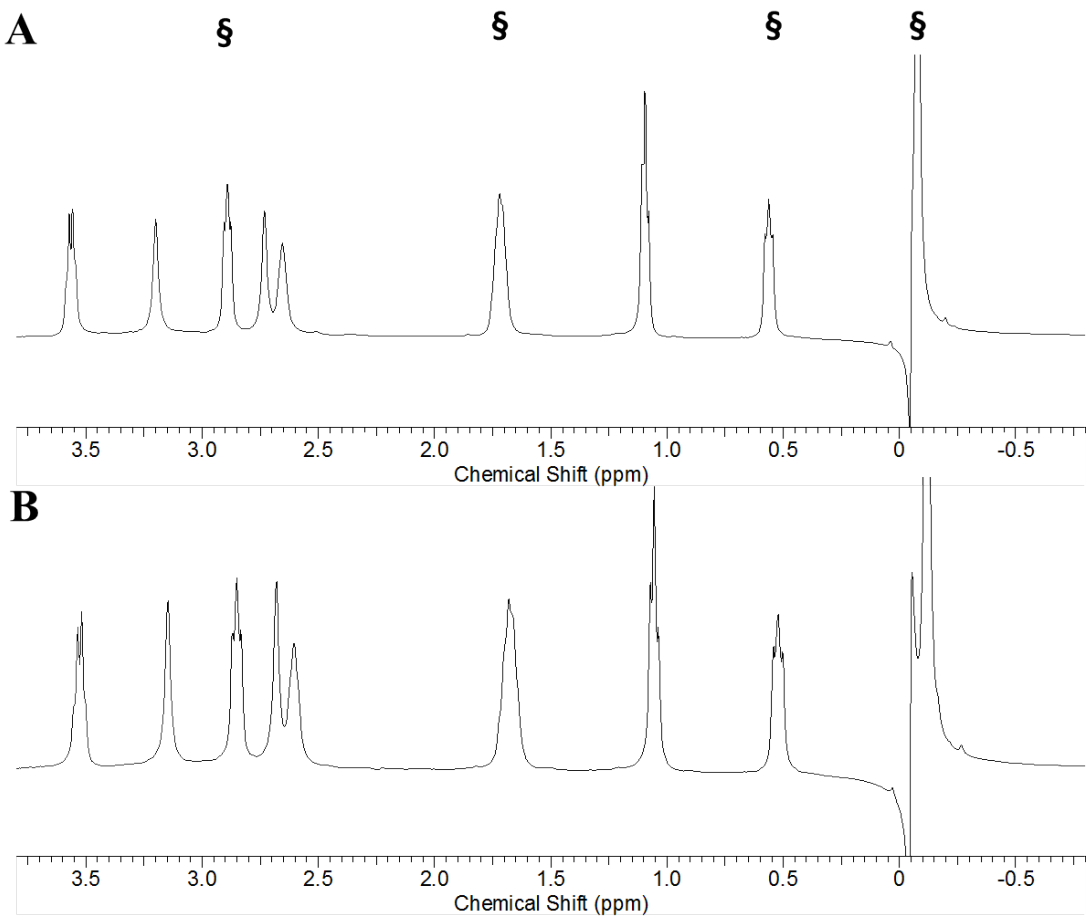


**Figure S7.** Diamagnetic region $^{1}$H NMR spectra of 10 mM $[Co(3)]^{2+}$,100 mM NaCl, 0.40 mM $Na_2HPO_4$, 25 mM $K_2CO_3$ in $D_2O$, pD 7.9 at 25 $^{o}$C (A) at 1 h (B) at 12 h after incubation at 37 $^{o}$C. Contains 5 mM 3-(trimethylsilyl)-1-propanesulfonic acid standard, indicated by §.

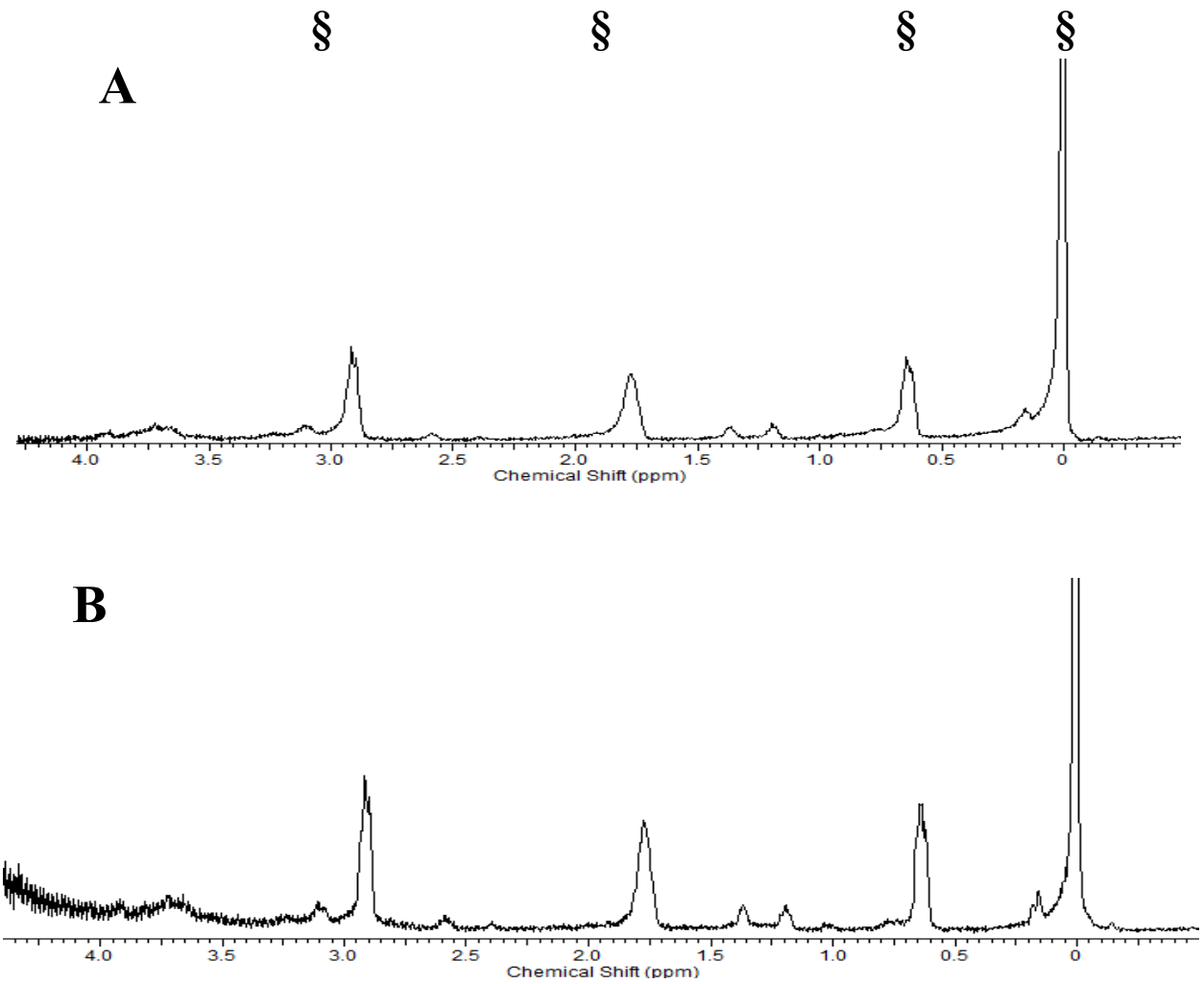


**Figure S8.** Diamagnetic region $^{1}$H NMR spectra of 10 mM $[Co(4)]^{2+}$,100 mM NaCl, 0.40 mM $Na_2HPO_4$, 25 mM $K_2CO_3$ in $D_2O$, pD 7.5 at 37 $^{o}$C (A) at 1 h (B) at 12 h after incubation at 37 $^{o}$C. Contains 5 mM 3-(trimethylsilyl)-1-propanesulfonic acid standard, indicated by §.

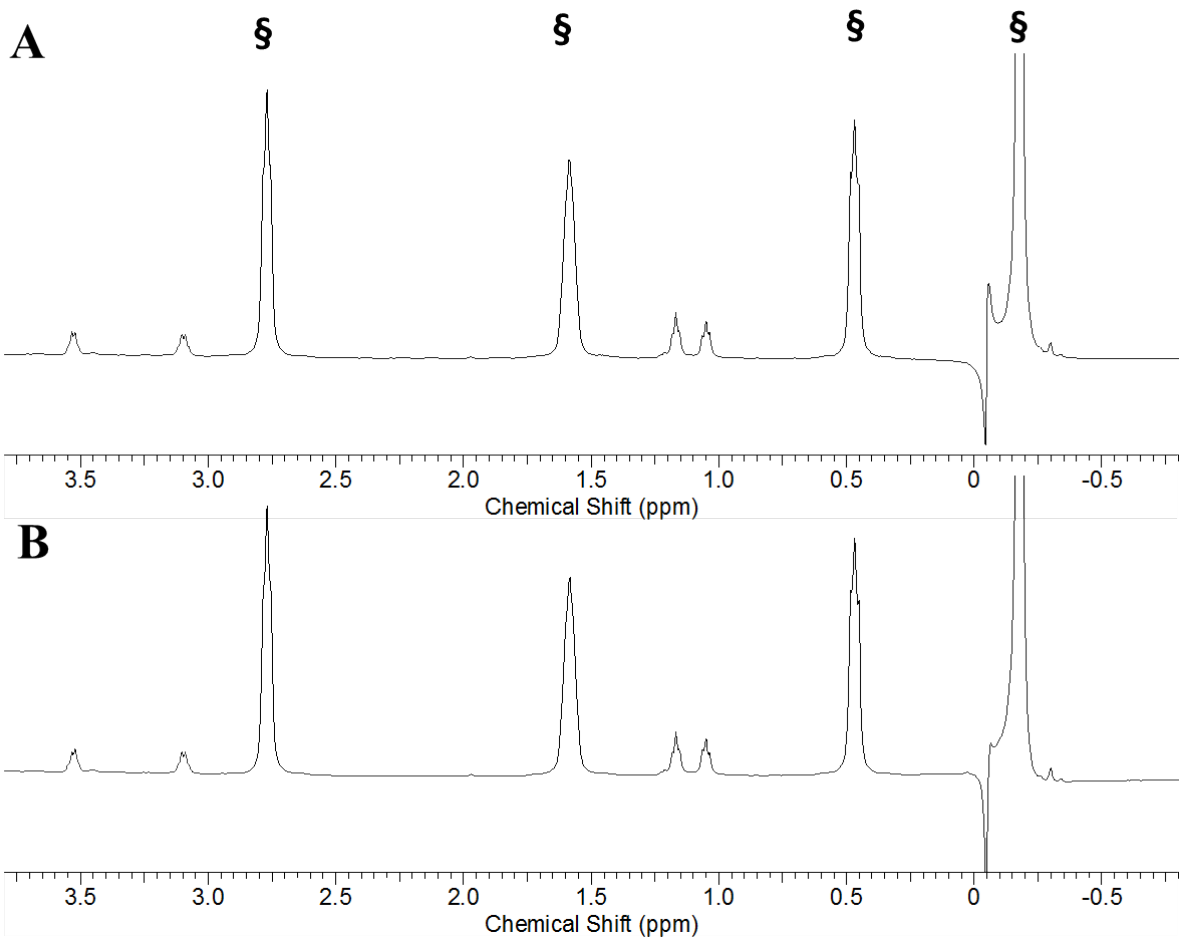


**Figure S9.** Diamagnetic region $^{1}$H NMR spectra of 10 mM $[Co(1)]^{2+}$,100 mM NaCl, in $D_2O$, pD 3.7 at 25 $^{o}$C (A) at 1 h (B) at 12 h after incubation at 37 $^{o}$C. Contains 5 mM 3-(trimethylsilyl)-1-propanesulfonic acid standard, indicated by §.

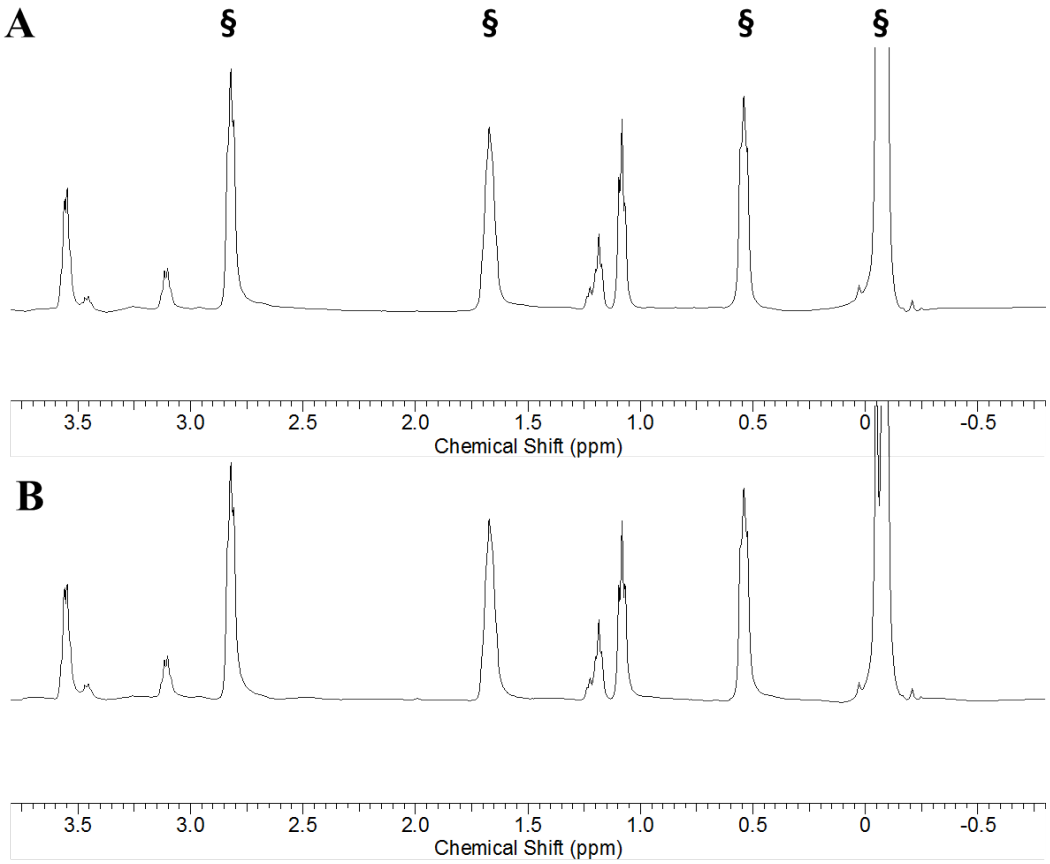


**Figure S10.** Diamagnetic region $^{1}$H NMR spectra of 10 mM $[Co(2)]^{2+}$,100 mM NaCl, in $D_2O$, pD 3.5 at 25 $^{o}$C (A) at 1 h (B) at 12 h after incubation at 37 $^{o}$C. Contains 5 mM 3-(trimethylsilyl)-1-propanesulfonic acid standard, indicated by §.

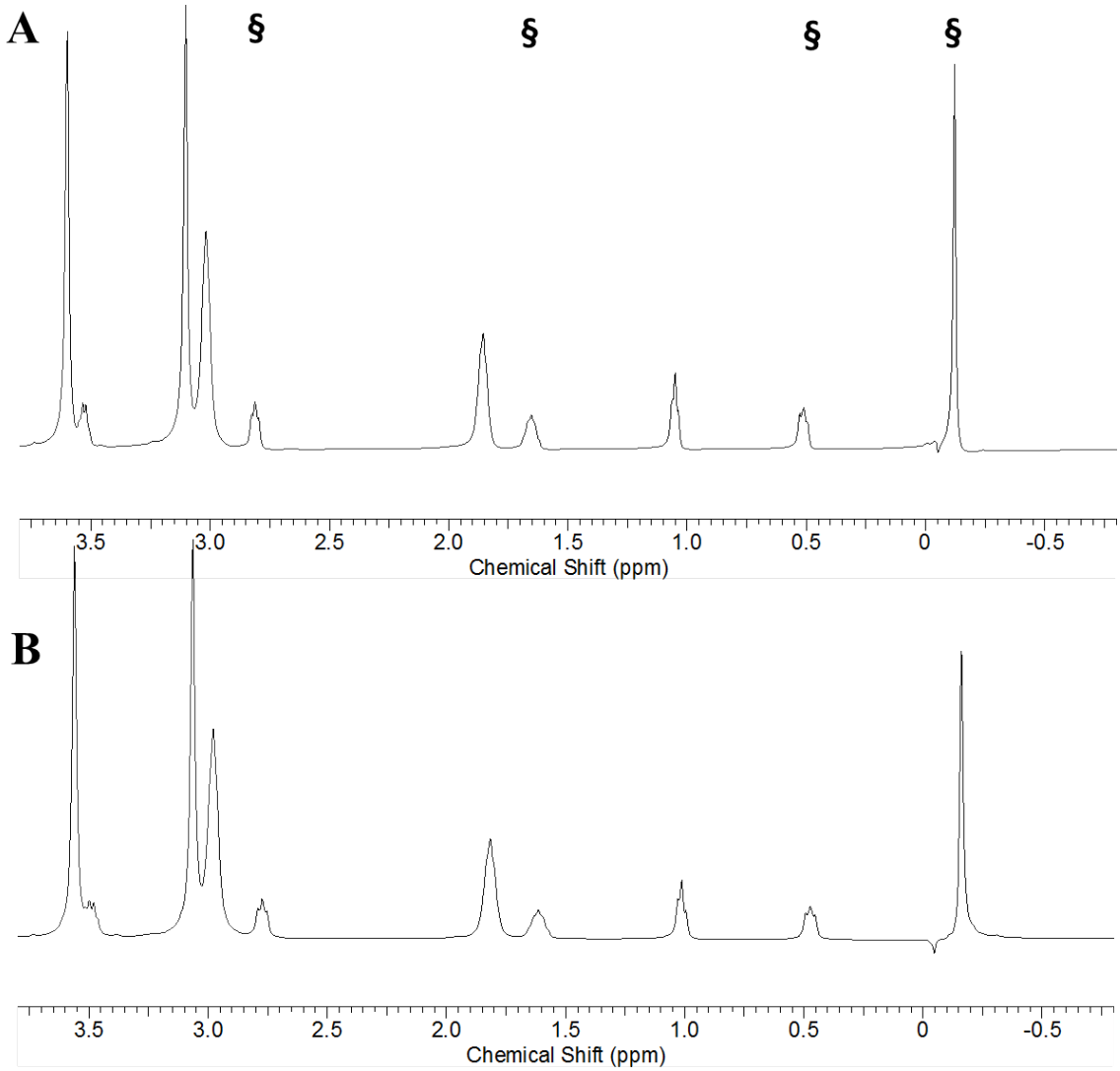


**Figure S11.** Diamagnetic region $^{1}$H NMR spectra of 10 mM $[Co(3)]^{2+}$,100 mM NaCl, in $D_2O$, pD 3.9 at 25 $^{o}$C (A) at 1 h (B) at 12 h after incubation at 37 $^{o}$C. Contains 5 mM 3-(trimethylsilyl)-1-propanesulfonic acid standard, indicated by §.

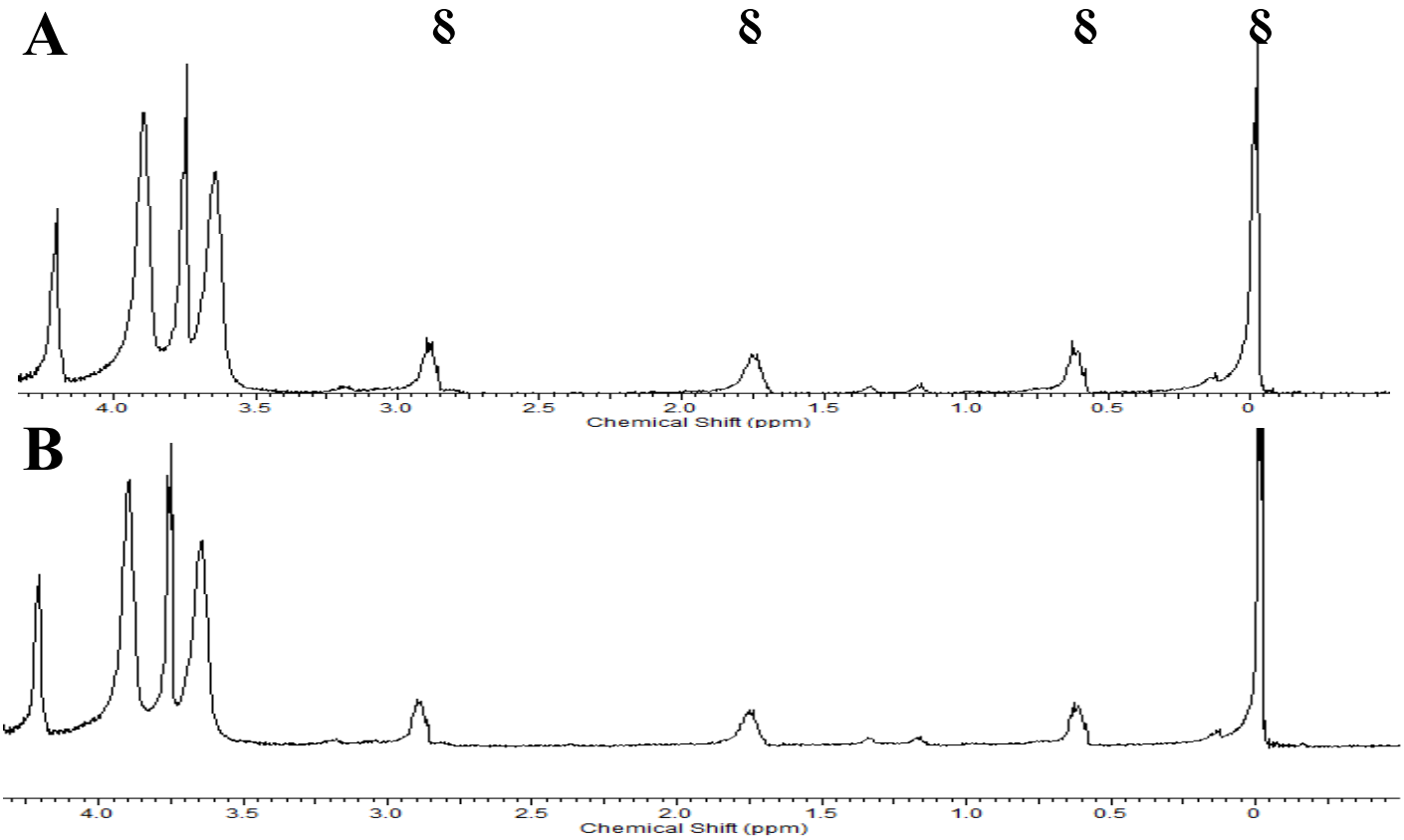


**Figure S12.** Diamagnetic region $^{1}$H NMR spectra of 10 mM $[Co(4)]^{2+}$,100 mM NaCl, in $D_2O$, pD 3.9 at 37 $^{o}$C (A) at 1 h (B) at 4 h after incubation at 37 $^{o}$C. Contains 5 mM 3-(trimethylsilyl)-1-propanesulfonic acid standard, indicated by §.

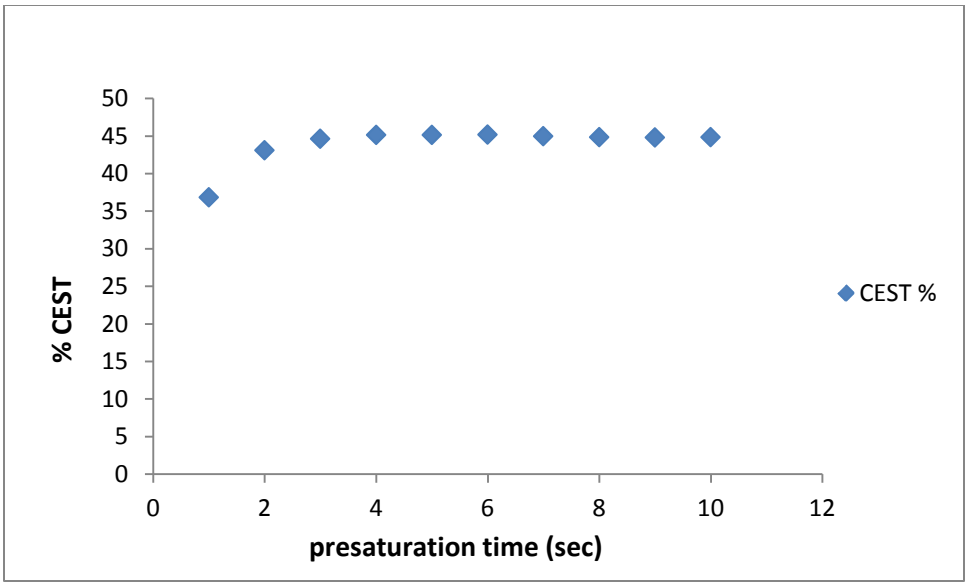


**Figure S13**. CEST recorded at 11.7 T of a solution of 10 mM $[Co(4)]^{2+}$, 100 mM NaCl, 20 mM HEPES pH = 7.4 at 37 ºC. RF presaturation pulse $B_1$ = 24 T was applied at different times (1-10 s).

**A**

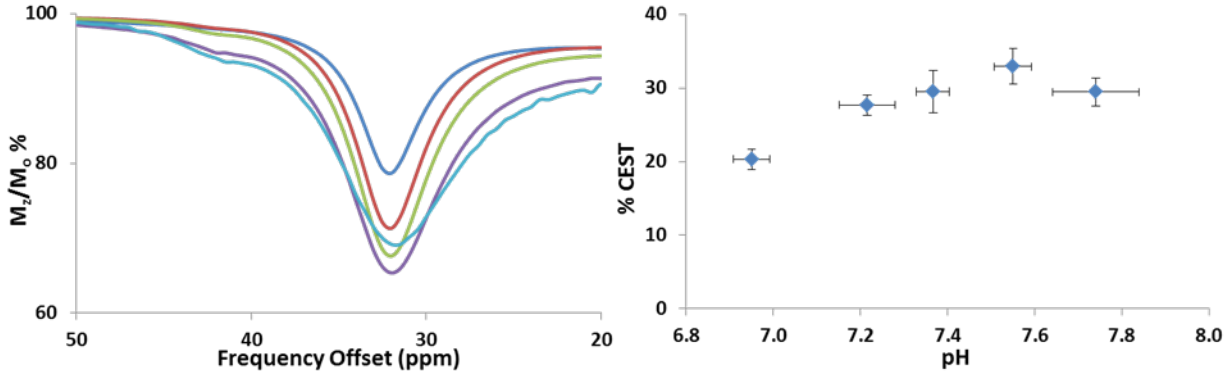
100
80
60
$M_z/M_o$ %
50
40
30
20
Frequency Offset (ppm)
40
30
20
10
0
% CEST
6.8
7.0
7.2
7.4
7.6
7.8
8.0
pH

**B**

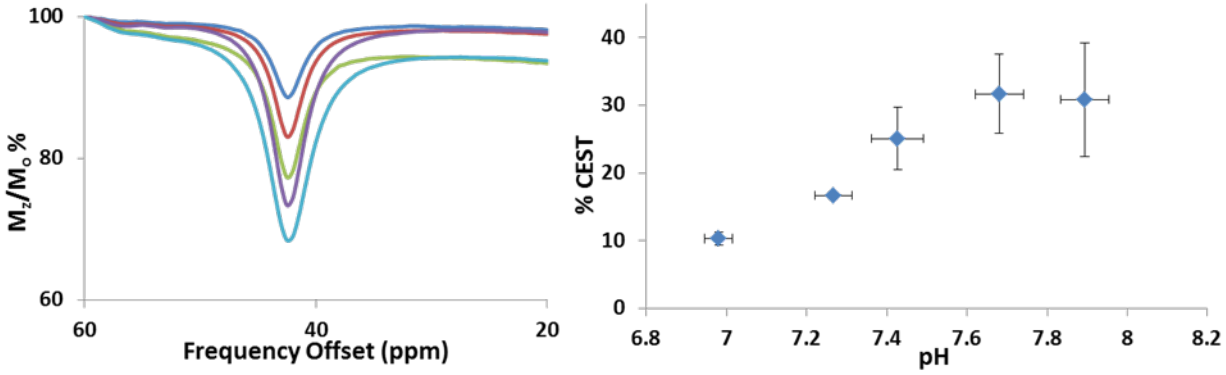
100
80
60
$M_z/M_o$ %
60
40
20
Frequency Offset (ppm)
40
30
20
10
0
% CEST
6.8
7
7.2
7.4
7.6
7.8
8
8.2
pH

**C**

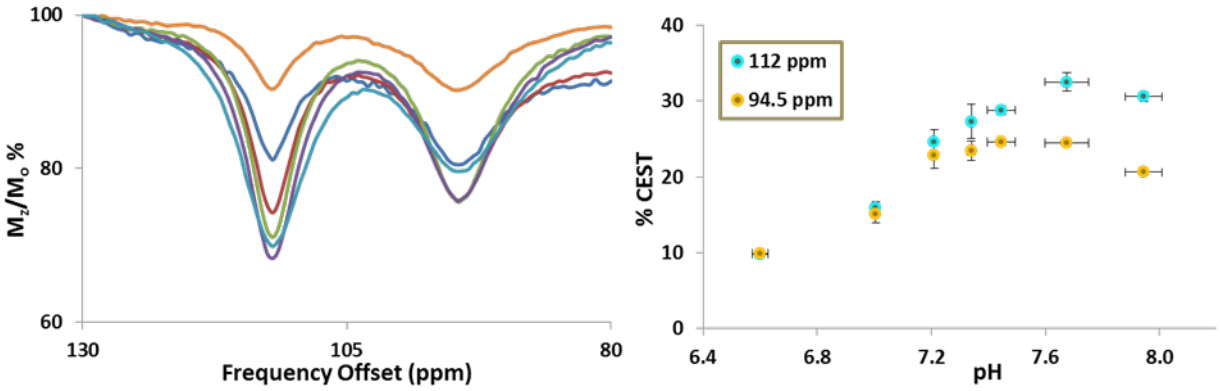
100
80
60
$M_z/M_o$ %
130
105
80
Frequency Offset (ppm)
40
30
20
10
0
% CEST
112 ppm
94.5 ppm
6.4
6.8
7.2
7.6
8.0
pH

**D**

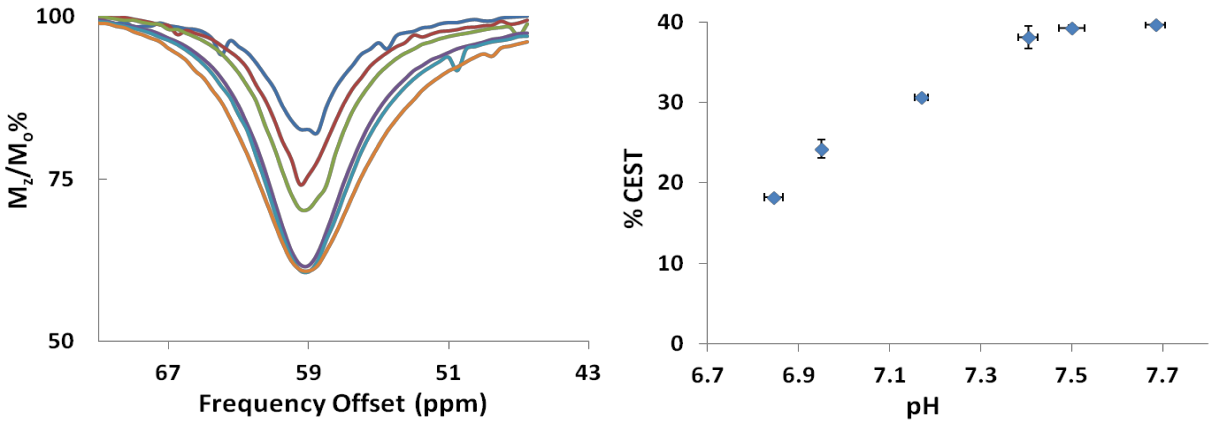


**Figure S14.** CEST recorded at 11.7 T of A) 10 mM $[Co(1)]^{2+}$; B) 10 mM $[Co(2)]^{2+}$; C) 10 mM $[Co(3)]^{2+}$; D) 10 mM $[Co(4)]^{2+}$; All solutions contained 20 mM buffer (pH 6.6 to 7.8) and 100 mM NaCl. RF presaturation pulse ($B_1$ = 24 μT) was applied for 2 s at 37 °C. Plot on the left shows the CEST peak shape in the region of exchange and plot on the right shows the maximum % CEST (depth of peak) over the pH range of pH 6.6 to 7.8. Error bars are for standard deviations for three measurements.

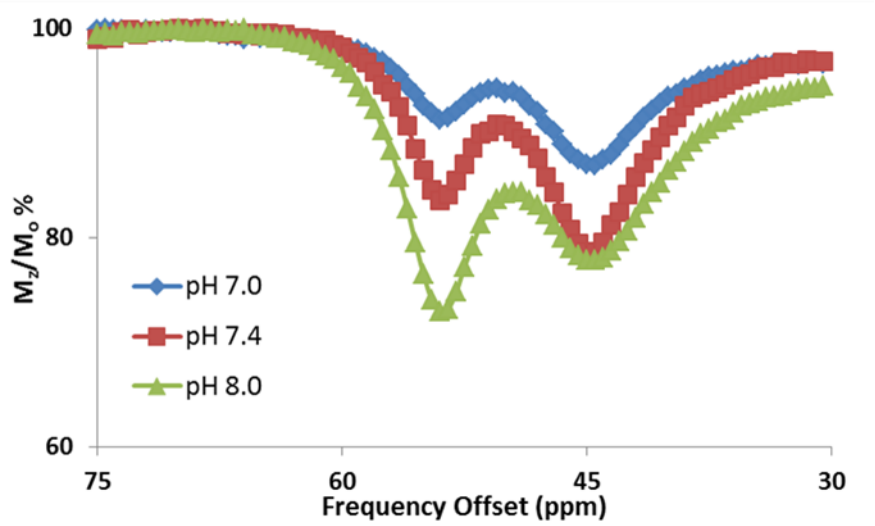


**Figure S15**. pH-dependence of 10 mM $[Co(3)]^{2+}$, 20 mM HEPES, 100 mM NaCl, 37 °C, CEST spectra of inner $[Co(3)]^{2+}$ peaks ($B_1$ = 1000 Hz, 2 s).

**Table S1**. $k_{ex}$ for $[Co(3)]^{2+}$ CEST peaks determined from the omega plot method for 10 mM $[Co(3)]^{2+}$, 20 mM HEPES, 100 mM NaCl, 37 °C, $B_1$ varies, 4 s.

| | $k_{ex}$ ($s^{-1}$) | | |
|---|---|---|---|
| | pH 7.0 | pH 7.4 | pH 8.0 |
| 112 ppm | 300 | 510 | 1550 |
| 95 ppm | 540 | 910 | 2100 |
| 54 ppm | 380 | 440 | 920 |
| 45ppm | 480 | 780 | 1760 |

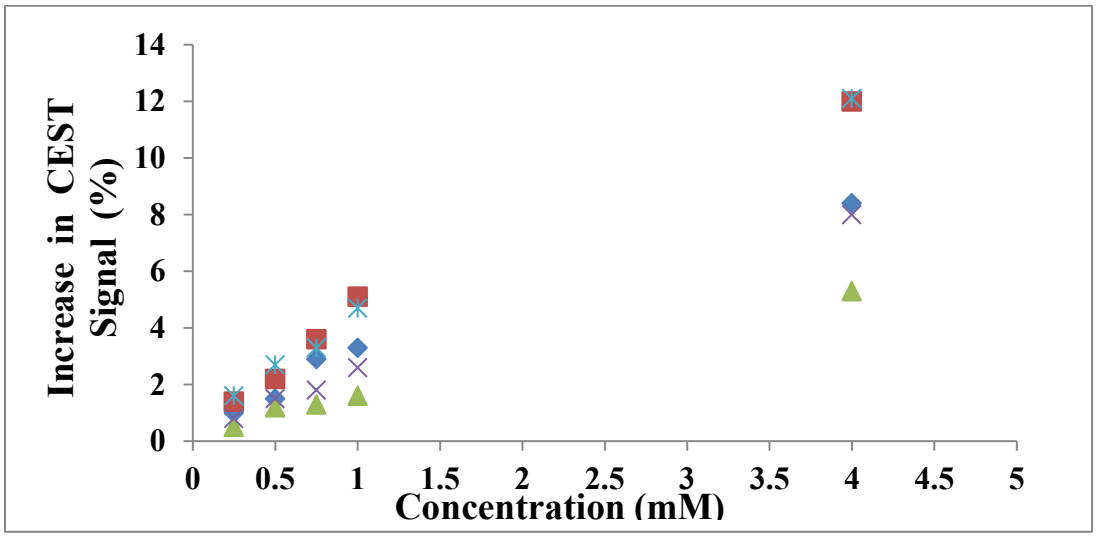


**Figure S16.** Plot of the increase in CEST signal 12 μT on 4.7 T MRI scanner of a solution containing 0.25 mM -4.00 mM $Co^{II}$ complexes (diamond = $[Co(1)]^{2+}$, square = $[Co(2)]^{2+}$, triangle = $[Co(3)]^{2+}$, X = $[Co(4)]^{2+}$), 100 mM NaCl , and 20 mM HEPES pH 7.4-7.5 at 37 °C.

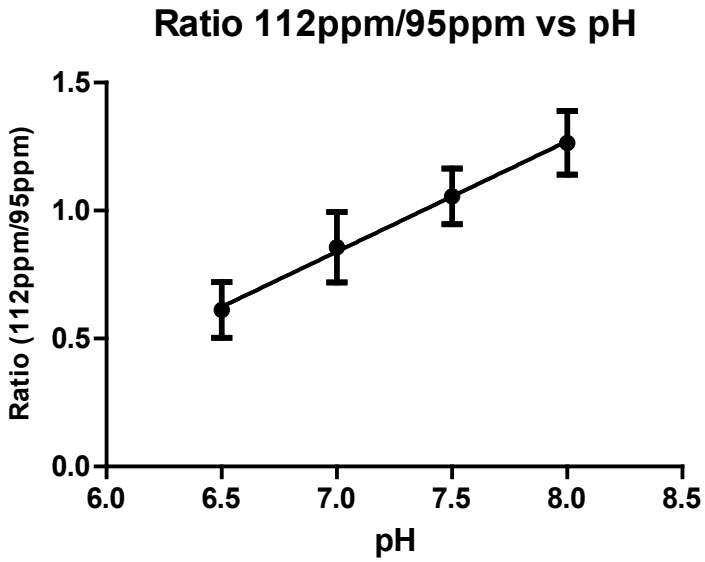


**Figure S17.** 4 mM samples of $[Co(3)]^{2+}$ containing 20 mM buffer (MES or HEPES),100 mM NaCl, at pH 6.5 – 8.0, plotted ratiometrically as % CEST at 112 ppm versus % CEST at 95 ppm. Recorded at 37 $^{o}$C using a CEST-FISP acquisition with a 5 x 1 s, 12 μT pulse train on a 4.7 T MRI scanner. A linear regression gives 0.43 for the slope of the line. Error bars are standard deviations from three measurments.

**References**


(1) Evans, D. F. *J. Chem. Soc.* **1959**, 2003.
(2) Schubert, E. M. *J. Chem. Ed.* **1992**, *69*, 62.
(3) Iskenderian, H. P. *Phys. Rev.* **1937**, *51*, 1092.
(4) Chin, K. O. A.; Morrow, J. R.; Lake, C. H.; Churchill, M. R. *Inorg. Chem.* **1994**, *33*, 656.
(5) Dixon, W. T.; Ren, J.; Lubag, A. J. M.; Ratnakar, J.; Vinogradov, E.; Hancu, I.; Lenkinski, R. E.; Sherry, A. D. *Magn. Reson. Med.* **2010**, *63*, 625.
(6) Dorazio, S. J.; Tsitovich, P. B.; Siters, K. E.; Spernyak, J. A.; Morrow, J. R. *J. Am. Chem. Soc.* **2011**, *133*, 14154.
(7) Amin, S.; Marks, C.; Toomey, L. M.; Churchill, M. R.; Morrow, J. R. *Inorganica Chim. Acta* **1996**, *246*, 99.
(8) Amin, S.; Morrow, J. R.; Lake, C. H.; Churchill, M. R. *Angew. Chem. Int. Ed. Engl.* **1994**, *33*, 773.
(9) Amin, S.; Voss, D. A., Jr.; Horrocks, W. D., Jr.; Lake, C. H.; Churchill, M. R.; Morrow, J. R. *Inorg. Chem.* **1995**, *34*, 3294.
(10) Dorazio, S. J.; Tsitovich, P. B.; Gardina, S. A.; Morrow, J. R. *J. Inorg. Biochem.* **2012**, *117*, 212.
(11) Olatunde, A. O.; Dorazio, S. J.; Spernyak, J. A.; Morrow, J. R. *J. Am. Chem. Soc.* **2012**.